EES Catalysis

PAPER

View Article Online
View Journal

Cite this: DOI: 10.1039/d6ey00007j

What formate electro-oxidation can teach us about CO poisoning on Pt during biomass oxidation

Silvia Favero, *[ab] Zhe Meng,[c] Henrik H. Kristoffersen, [c] Jan Rossmeisl, [c] Ifan E. L. Stephens, [d] Maria Magdalena Titirici [ae] and Yu Katayama *[b]

Received 7th January 2026,
Accepted 6th March 2026

DOI: 10.1039/d6ey00007j

rsc.li/eescatalysis

Catalyst deactivation by *CO poisoning remains a central challenge in the electrochemical oxidation of biomass-derived molecules such as glycerol and glucose. On platinum catalysts, *CO forms readily as a reaction intermediate, blocking active sites and requiring high overpotentials for removal—often leading to undesired overoxidation of valuable products. Understanding the fundamental origins of *CO formation is thus critical for designing more selective and stable catalysts. Here, we employ formate oxidation as a model system to study CO formation on Pt in alkaline media. Using *operando* surface-enhanced infrared absorption spectroscopy, we show that the adsorption configuration of formate governs whether CO poisoning occurs. Oxygen-bound formate (*OOCH) undergoes stable direct oxidation to CO_2, whereas carbon-bound formate-derived species, consistent with *COOH, disproportionate to form *CO–*OH and initiate surface poisoning. These findings provide a mechanistic framework for suppressing CO formation on Pt by selectively stabilizing oxygen-bound intermediates, with broader implications for improving the performance of biomass electrooxidation reactions.

Broader context

Electrochemical oxidation reactions are central to sustainable energy and chemical technologies, including low-temperature fuel cells, hydrogen co-production, and the conversion of biomass into valuable chemicals. A major obstacle to their widespread application is catalyst deactivation, particularly on platinum, where strongly adsorbed carbon monoxide (*CO) blocks active sites and reduces efficiency. Understanding how and why *CO forms is therefore a critical challenge with implications for energy conversion, green chemistry, and industrial electrocatalysis. Formic acid oxidation provides a simplified model system to study this problem, yet most existing knowledge is derived from acidic conditions, even though many practical oxidation processes operate in alkaline media. In this work, we use *operando* infrared spectroscopy to directly track surface intermediates during formate oxidation in alkaline electrolyte. We show that the way formate binds to the catalyst surface determines whether the reaction proceeds *via* the direct and stable oxidation to CO_2 or leads to *CO poisoning. By identifying adsorption geometry as a key control parameter, this study offers design principles for developing more durable catalysts, with relevance extending beyond formic acid to a wide range of biomass-derived oxidation reactions.

Introduction

Formic acid oxidation is an attractive electrocatalytic reaction, having been explored for direct formic acid fuel cells and for on-demand electricity generation due to its high theoretical efficiency, and mild operating conditions. Beyond these applications, the electrochemical oxidation of formic acid on platinum has long served as a prototypical system for studying small-molecule electrocatalysis. Formic acid is intrinsically interesting because its oxidation involves a limited number of well-defined surface intermediates and proceeds through two parallel mechanisms, one of which produces *CO, a canonical poisoning species. Despite its apparent simplicity, formic acid oxidation remains mechanistically rich, exhibiting both direct and indirect pathways that depend sensitively on surface structure, potential, and electrolyte composition.

Formic acid oxidation has been extensively investigated, particularly in acidic media,[1–12] yet several gaps remain in our understanding. *Operando* and surface-sensitive spectroscopic

[a] *Imperial College London, Chemical Engineering Department, South Kensington Campus, London, SW72AZ, UK. E-mail: silvia.favero@icn2.cat*
[b] *SANKEN, The University of Osaka, Osaka, 567-0047, Japan. E-mail: yuktym@sanken.osaka-u.ac.jp*
[c] *Department of Chemistry, University of Copenhagen, Universitetsparken 5, Copenhagen 2100, Denmark*
[d] *Imperial College London, Materials department, Molecular Sciences Research Hub, London, W12 0BZ, UK*
[e] *Advanced Institute for Materials Research, Tohoku University, Sendai, Japan*

techniques, such as surface-enhanced infrared absorption spectroscopy (SEIRAS), are essential for identifying adsorbates in real time, as conventional electrochemical measurements cannot resolve individual intermediates. To date, the only intermediates that have been directly observed experimentally by SEIRAS are bidentate (bridge-bonded) formate (*OOCH) and adsorbed *CO, and their vibrational signatures are well documented.[2,6,12,13] However, density functional theory (DFT) calculations suggest that bidentate formate is too stable to account for the observed reactivity,[14] while experimental studies report only limited correlations between *OOCH coverage and either the rate of oxidation or the onset of *CO formation.[9] Together, these observations strongly imply the existence of an additional, yet unobserved, reactive intermediate.

A key advantage of formic acid oxidation is that it provides a simplified platform for mechanistic analysis by *in situ* vibrational spectroscopy. Assigning specific infrared bands to individual intermediates remains challenging in complex biomass oxidation reactions, as infrared spectroscopy probes vibrational modes associated with changes in the dipole moment of adsorbed species. In reactions such as glycerol oxidation, many common products and intermediates—including carboxylates, aldehydes, ketones, acyl groups, and carbonates—exhibit overlapping bands in the 1100–1750 cm^{-1} region, making unambiguous peak assignment difficult. As highlighted in our recent review on the challenges of glycerol oxidation,[15] this spectral congestion is a general limitation of biomass electrooxidation studies. Moreover, adsorption to the catalyst surface can significantly shift vibrational frequencies relative to solution-phase species, rendering *ex situ* product analysis insufficient for identifying intermediates observed *in situ*. While DFT calculations can assist by predicting vibrational frequencies, these predictions alone are often insufficient to distinguish closely related species, such as the COO stretching modes of lactic acid, glycolic acid, and glyceric acid. In contrast, formic acid oxidation involves a much smaller number of plausible intermediates, enabling clearer correlation between spectroscopic features, adsorption geometries, and reaction pathways.

Fig. 1 summarizes the pathways for the direct (blue) and indirect (orange) oxidation of formic acid, that have been previously proposed in literature. Initially, the direct pathway was attributed to bidentate formate (adsorbate 1 in Fig. 1, bound through two oxygen atoms) by Samjeske *et al.*[2,12] and Cuesta *et al.*,[7,8] following SEIRAS measurements in acidic media that correlated bidentate formate with direct oxidation. However, subsequent experimental evidence revealed that the direct oxidation mechanism is more complex. The current measured is not proportional to the coverage of adsorbed bidentate formate,[9] and adsorbed bisulfates, which reduce bidentate formate coverage, can enhance the reaction rate.[16] DFT simulations further indicate that C–H bond cleavage from bidentate formate requires a high activation energy,[14] whereas the same step is energetically more favorable for monodentate formate adsorbed *via* one oxygen atom (species 3 in Fig. 1).[6] This led to the proposal that monodentate *OOCH might be the reactive species.[6,11] However, this hypothesis conflicts with spectroscopic observations[2,12,13] and with other DFT studies showing that the bidentate configuration is approximately

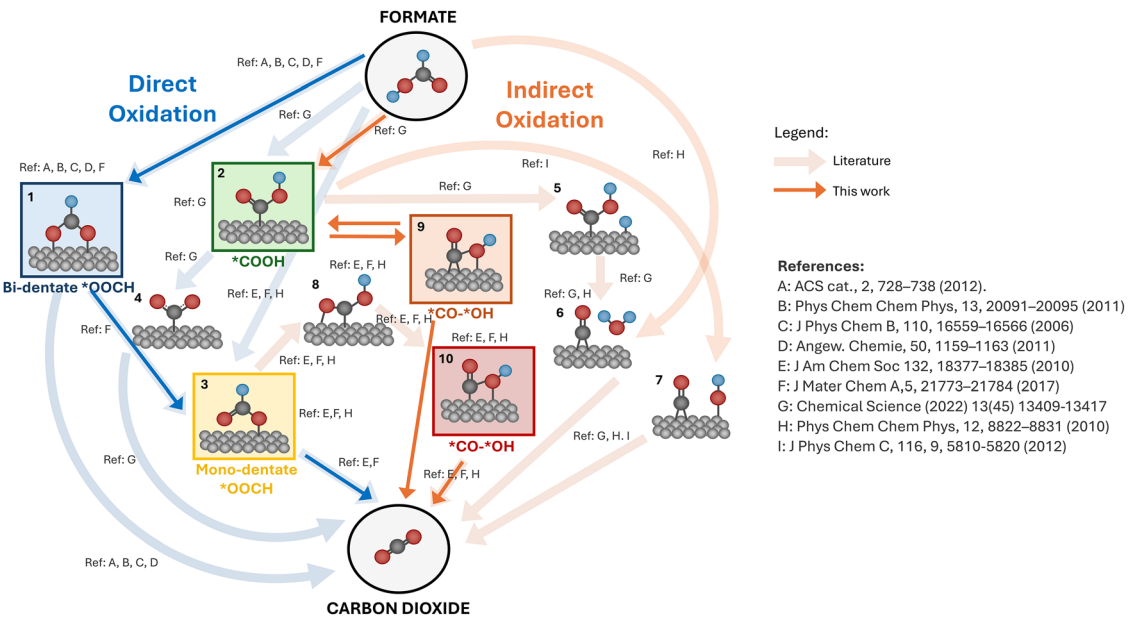

Fig. 1 Schematics of the mechanisms of formic acid oxidation proposed in the literature (semi-transparent arrows). In blue are shown the mechanism for direct oxidation, while in orange are shown the mechanisms proposed for indirect oxidation, through the formation of carbon monoxide. The mechanism suggested in this work is highlighted with full arrows and boxes around the proposed intermediates: bidentate *OOCH (in blue), monodentate *OOCH (in yellow), *COOH (in green), bridge-bonded *CO–*OH (in orange) and linear bonded *CO–*OH (in red). All these intermediates, except monodentate *OOCH, are detected by SEIRAS. Monodentate *OOCH is reported to be only stable in pockets of bi-dentate *OOCH[6] and to be easily oxidized, leading to short residence times and very low coverages, explaining the lack of SEIRAS detection.

0.7 eV more stable.[6] Herrero and co-workers reconciled these findings by proposing that adsorption of bidentate formate creates local environments in which monodentate *OOCH can transiently form and undergo C–H cleavage with minimal activation energy.[6] Nevertheless, this mechanism has not been experimentally confirmed, and alternative DFT studies indicate that other intermediates, including *COOH (species 2 in Fig. 1), may play a central role in both direct and indirect oxidation pathways.[3] Other reports have proposed monodentate formic acid as the active species, while bidentate *OOCH may act as a spectator or even inhibit the reaction.[11]

Kwon *et al.* showed that formic acid oxidation on Pt has a strong pH dependence, with the maximum in current density located at the pK_a of formic acid. They proposed that the reaction proceeds through the oxidation of formate, rather than formic acid, explaining the positive effect of increasing the pH from 0 to 4.[13] At higher pH, activity decreases due to increasing competition with *OH adsorption. Despite the crucial role of pH, most fundamental mechanistic studies on formic acid or formate oxidation continue to focus on acidic media, leaving significant scope for insight from alkaline conditions. In this work, we will use the terms formic and formate oxidation, when referring to this reaction in acidic and alkaline pH respectively.

The pathway for indirect oxidation remains similarly debated. Several studies suggest that direct and indirect oxidation may share common intermediates,[3,17] and that *CO formation appears site demanding.[6,18–20] Bagger *et al.* have proposed that *CO formation happens through the disproportionation reaction of *COOH and requires the presence of adsorbed protons (pathway following species 2, 5 and 6 in Fig. 1).[3] The requirement of *H was shown experimentally by the increase in the anodic activity, when the lower limit of the cyclic voltammogram is increased, with cycles completed between 0.4 and 1 V *vs.* RHE showing no hysteresis.[3] However, studying stepped Pt surfaces, Feliu and co-workers reported that *CO formation does not happen in the HUPD region, but rather around the potential of zero total charge, where both protons and anions adsorptions are favoured but neither dominate.[10,21] In line with these observations, it has been proposed that indirect oxidation starts from monodentate adsorbed formate (*OOCH) and proceed through a formate intermediate where both the carbon and the oxygen are adsorbed (species 8 in Fig. 1), in a mechanism that requires both protons and OH.[5,6]

Adding to this complexity, *CO vibrational bands during the oxidation of small organic molecules and biomass-derived substrates have been reported at frequencies significantly lower than expected from CO adsorption.[22] The origin of these red-shifted *CO species remains unclear and is frequently attributed empirically to coverage effects or coadsorbate interactions, without a clear mechanistic basis.

In this work, we address these open questions by using *operando* SEIRAS to study formate oxidation on Pt in alkaline media. We identify two distinct formate-derived intermediates: the well-established bidentate *OOCH, which dominates under conditions of stable direct oxidation, and a second intermediate, most consistent with a carbon-bound formate-derived species, which correlates directly with *CO formation. By explicitly linking adsorption geometry to reaction outcome, our results enable the derivation of design criteria to suppress *CO poisoning, namely by favoring oxygen-bound intermediates over carbon-bound pathways. These insights are directly relevant to other electrocatalytic oxidation reactions where *CO formation limits performance, including glycerol,[23–25] glucose,[26,27] and alcohol oxidation[28] on platinum, in which formate- or formyl-like intermediates are commonly implicated.

Results

SEIRAS results and peak assignment

Fig. 2a shows the cyclic voltammogram (CV) of polycrystalline Pt in alkaline electrolyte in the presence of formate (1 M formate, 1 M NaOH). This scan shows a hysteresis between the anodic and cathodic peaks, typical of the electrooxidation of formate on Pt.[3–5,13,29–35] In particular, in the anodic scan, the oxidation current peaks at around 0.35 V (peak 1) and then starts to drop, followed by a sharper peak at 0.6 V *vs.* RHE (peak 2). On the cathodic scan, the current reaches a higher peak at 0.4 V *vs.* RHE (peak 3). Fig. 2b shows the results of *operando* SEIRAS measurements, as a function of time and applied potential. From the bottom to the top of the graph, data are shown for increasing time. The orange lines at the bottom show the stable background (in 1 M NaOH, at OCP) before the addition of formate, light orange lines show the change in the spectra after the addition of 1 M formate, at open circuit potential (0.9 V *vs.* RHE). Then, cyclic voltammetry is performed between 1 and 0 V *vs.* RHE, shown in colors ranging from purple to yellow. Spectra are color-coded to match the potential of the cyclic voltammogram in Fig. 2a.

At OCP, 4 peaks can be observed at 1630 cm^{-1}, 1590 cm^{-1}, 1380 cm^{-1}, 1350 cm^{-1}. The peak at 1630 cm^{-1} is assigned to interfacial water,[34] while the remaining ones are assigned to the C–H and C=O (symmetric and asymmetric) stretching of formate in solution (Fig. 2b).[36,37] Starting from 0.6 V *vs.* RHE, in concomitance with the detection of an anodic current, new peaks appear, caused by the formation of new adsorbate. Two peaks are first observed at 1440–1460 cm^{-1} and 1270–1290 cm^{-1}. In literature, a band between 1320 to 1350 cm^{-1} has been reported and consistently assigned to the symmetric O–C–O stretching mode of bidentate (bridge-bonded) *OOCH.[2,7,12,13,34] The corresponding asymmetric stretch is typically weak or absent in SEIRAS due to the surface-selection rule, which enhances only vibrations that involve dipole changes normal to the metal surface. To confirm the assignments, we performed density functional theory (DFT) calculations of the vibrational frequencies of the relevant intermediates (Fig. 3). For bidentate *OOCH, DFT predicts modes at 1305 cm^{-1} (symmetric O–C–O stretch) and 1555 cm^{-1} (asymmetric O–C–O stretch), in good agreement with earlier works.[2,13,34]

In this work, we observe a band at 1440–1460 cm^{-1}, which we assign to the symmetric O–C–O stretch of bidentate *OOCH.

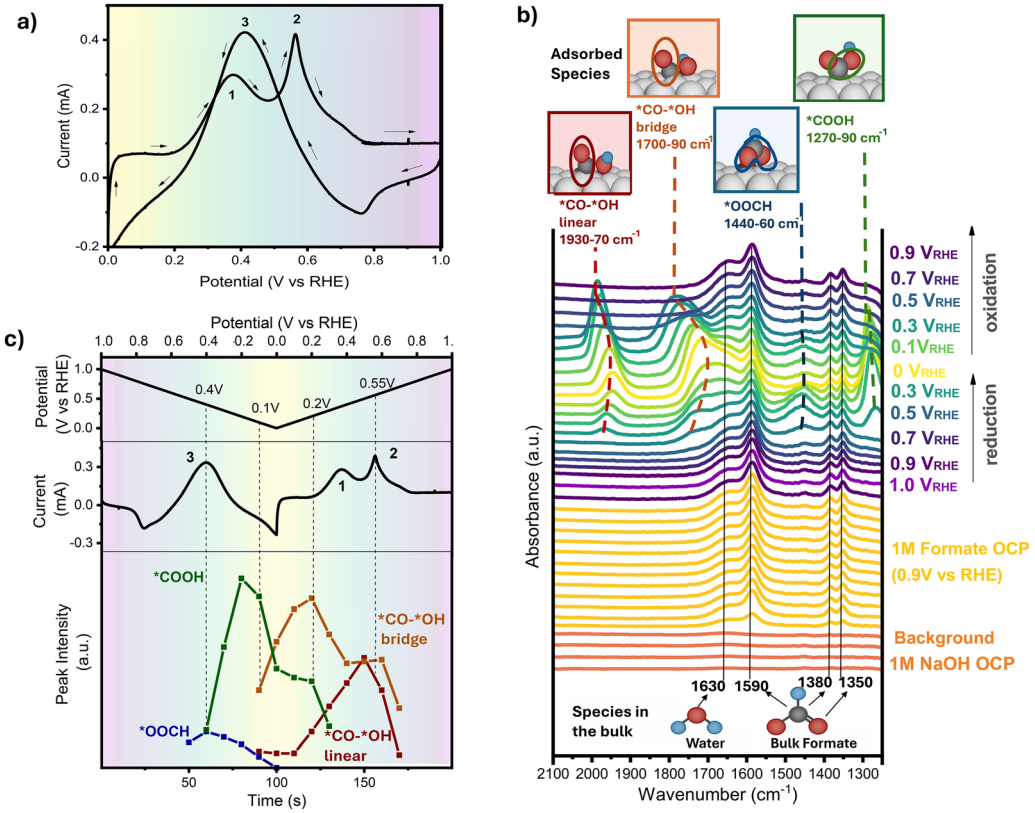

Fig. 2 (a) cyclic voltammogram in 1 M NaOH and 1 M formate. The cycle starts at OCP (0.9 V *vs.* RHE), then the potential is scanned anodically up to 1 V *vs.* RHE and cathodically to 0 V *vs.* RHE, at a scan rate of 10 mV s^{-1}. Data were collected in an *in situ* cell, described in the experimental section, at 25 °C. The working electrode is polycrystalline Pt deposited on a Si optical prism (b) background-subtracted *in situ* surface-enhanced FTIR spectra, collected during the cyclic voltammogram shown in part a. The time increases from the bottom to the top of the graph. The background was collected at OCP in 1 M NaOH (orange curves at the bottom of the graph), then formic acid was added and spectra were collected at OCP (light orange curves). Finally, the potential was cycled as described in part a and the spectra are color-coded according to the applied potential (with the same colours reported in the cyclic voltammogram). (c) The applied potential and current are shown in black, as a function of time. The intensity of the peaks observed observed in b is also reported as a function of time.

This frequency is slightly higher than previous experimental reports and DFT predictions. We attribute this blue-shift to the alkaline environment with high Na^+ concentration, which could coordinate to the adsorbate, stiffen the O–C–O bonds, modify the adsorption geometry, and induce lateral dipole–dipole interactions, all of which might increase the vibrational frequency. A blue-shift of similar intermediates in presence of cations has been observed before,[38,39] even though it has not been explicitly reported in electrocatalysis. Other electrostatic interactions could equally be responsible for the observed blue-shift, and dedicated cation-variation studies would be necessary to confirm the role of cations. Nevertheless, the origin of the blue shift does not affect the conclusions of this work. We also note that the band at 1440–1460 cm^{-1} is also close to the spectral signature of carbonate in alkaline media. However, we discard this assignment for three reasons: (i) the peak position of the intermediate observed here changes with potential, which is the typical behaviour of a surface bound species (ii) the band intensity is not proportional to the current, (iii) the same 1440–1460 cm^{-1} peak has been reported in presence of acetate, which is not oxidized by platinum and therefore does not produce carbonate.[40]

In this work, we also observe a second band at 1270–1290 cm^{-1}. Its formation and decay do not correlate with the 1440–1460 cm^{-1} band, which indicates that it arises from a different adsorbed species, rather than the symmetric stretch of bidentate *OOCH. Notably, a band in this region has not been unambiguously assigned or systematically discussed in prior SEIRAS studies of formic acid oxidation on Pt.

The 1270–1290 cm^{-1} feature could, in principle, correspond to a monodentate formate species bound through oxygen (*OCHO) or through carbon (*COOH), because both geometries can exhibit lower-frequency C–O stretching modes compared to bidentate *OOCH. In monodentate formate, only one oxygen atom interacts with the surface, which one could expect to reduce the O–C–O bond order and shift the OCO stretching frequency downward. In addition, monodentate adsorption geometries can produce a larger perpendicular dipole moment change for certain lower-frequency modes, making them SEIRAS-active even when the symmetric bidentate stretch is weak or undetectable according to the surface-selection rule. Nevertheless, monodentate formate has never been experimentally observed by SEIRAS on Pt, despite extensive studies in

a) SPECTROSCOPY-DETECTED ADSORBATES

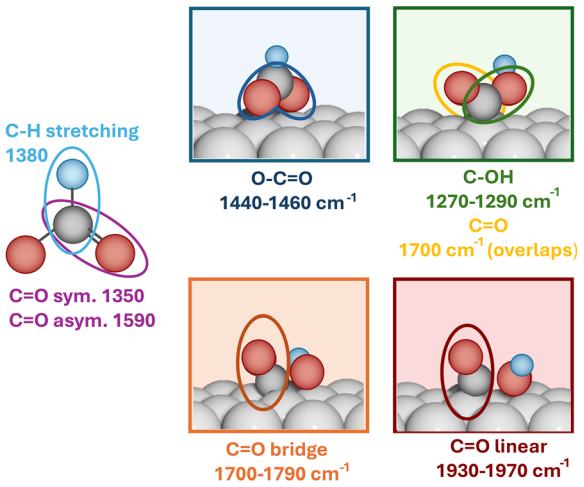

b) DFT PREDICTIONS OF VIBRATIONAL FREQUENCIES

Adsorbate	Mode	Experimental	DFT
*COOH	C-OH asymmetric stretching	1270-1290	1189
*COOH	C=O asymmetric stretching	NA (overlapping)	1686
*OOCH (bidentate)	O-C-O asymmetric stretching	NA (surface selection rule)	1555
	O-C-O symmetric stretching	1440-1460	1305
*CO (bridge)	C=O stretching	1830-1870 (from CO gas)	1820
*CO-*OH (bridge)	C=O stretching	1700-1790	1718-1810 (see Fig 6)
*CO (linear)	C=O stretching	2010-2050 (from CO gas)	2019
*CO-*OH (linear)	C=O stretching	1930-1970	1770-1990 (see Fig 6)
*CO (FCC)	C=O stretching	Not observed	1717

Fig. 3 (a) Summary of the IR peaks assignments, with DFT-optimized structure of the proposed intermediates and (b) the experimental and DFT predicted vibrational frequencies of the proposed intermediates. Details of the DFT simulations can be found in the "methods" section.

acidic media. Monodentate formate is also expected to be highly reactive and short-lived, and multiple mechanistic studies identify it as the key intermediate of the direct pathway of formic acid/formate oxidation.[5,6] Its instability provides a consistent explanation for why it has not been detected spectroscopically. Importantly, in the potential regions where the direct oxidation pathway is active and stable, we do not observe the 1270–1290 cm^{-1} band. This further argues against assigning this species to monodentate formate, although this possibility cannot be excluded.

*CO formation on Pt has been widely attributed to a C-bound *COOH intermediate, based on DFT calculations, single-crystal studies, and mechanistic modeling.[1,3,5,6] This assignment is rationalized because *COOH is sufficiently reactive to decompose into *CO while being formed at potentials consistent with CO generation, whereas bidentate formate is too stable and monodentate formate too short-lived to account for CO formation. However, to the best of our knowledge *COOH has not been directly observed by SEIRAS or ATR-FTIR, and its presence has only been inferred. The likely reasons for its absence in previous experiments are its short lifetime and the surface-selection rule. In our measurements, the high cation concentration in alkaline solution may stabilize this species and enhance its vibrational intensity, allowing us to detect it as the 1270–1290 cm^{-1} band.

To support this assignment, we also calculate the DFT-predicted vibrational frequencies for *COOH (Fig. 3), which are determined as 1189 cm^{-1} and 1686 cm^{-1} for the C–OH and C═O bond asymmetric stretching modes, respectively. Other frequencies for *COOH structure can be found in SI Table S1. The 1686 cm^{-1} frequency can't be detected from experiments because the frequency would overlap with the experimental strong bulk water (1630 cm^{-1}).

It should be noticed that, in alkaline conditions, formic acid is almost fully dissociated into formate, making direct adsorption of protonated formic acid to *COOH thermodynamically unlikely. A more likely possibility is that *COOH might be formed by the isomerization of monodentate *OOCH, as proposed by Herrero's,[5,6] and Mavrikakis's groups.[1] Another possibility is that the observed species might not be a true *COOH but rather a cation-stabilized formate, coordinated *via* the oxygen to Na^+ (O═C–O···Na^+).[5,6] Such a structure would exhibit similar vibrational characteristics to *COOH but cannot currently be reliably simulated with DFT.

Finally, at potentials of around 0.2 V, two very sharp peaks appear at 1700–1790 cm^{-1}, and at 1930–1970 cm^{-1}. These peaks are located in the CO adsorption region, but are around 100 cm^{-1} lower than those observed in CO-saturated NaOH, which are caused by the characteristic C≡O stretching mode of linear-bonded (2010–2060 cm^{-1}) and bridge-bonded (1830–1870 cm^{-1}) *CO.[34,35] This suggests that the *CO species observed here are partially hydrated (*i.e.* bound to a neighbouring *OH species, and here denoted as *CO–*OH), as shown in Fig. 3b and discussed in more details later. Additionally, we highlight the site preference for CO adsorption. As shown in Table S3, *CO adsorbing on Pt surface *via* fcc (hollow, ΔE = 0.32 eV, referenced to *COOH = 0 eV) site is energetically favored compared with bridge (ΔE = 0.35 eV) or linear (ΔE = 0.42 eV) configurations. However, experimental observations on Pt(111) surfaces indicate the presence of only bridge and linearly bonded *CO; this discrepancy between theory and

experiments is consistent with the literature for *CO binding on Pt(111).[41,42]

Tracking of potential-dependent intermediates' formation with SEIRAS

To better track the formation of the reaction intermediates, Fig. 2c shows the intensity of each adsorbate as a function of time and applied potential. From now on, the peaks at 1440–1460 cm^{-1} and 1270–1290 cm^{-1} will be referred to as *OOCH (O-bonded bidentate formate) and *COOH (C-bonded formic acid) respectively.

When scanning in the cathodic direction, first no reaction is detected due to *OH poisoning,[2,12,13,33] then a positive current is observed below 0.6 V *vs.* RHE (peak 3), which is accompanied by first the formation of a small amount of O-bonded formate (*OOCH), followed by the rapid formation of C-bonded formic acid (*COOH). At 0.2 V *vs.* RHE, the current becomes negative, indicating the formation of *H, accompanied by the formation of *CO bridge and the consumption of *COOH. In the anodic scan, the current positive of 0.2 V *vs.* RHE (peak 1) is accompanied by an increase in *CO linear, a decrease in *CO bridge and the disappearance of *COOH. Finally, at 0.6 V *vs.* RHE, in conjunction with peak 2, both the bridge and linear *CO are consumed.

These results suggest that the O-bonded formate is responsible for the direct oxidation pathway and C-bonded formic acid is responsible for the indirect oxidation pathway. In the cathodic scan, the presence of only the *OOCH intermediate in the rising side of peak 3 suggests that *OOCH is responsible for the direct oxidation pathway. We note that previous DFT simulations have shown that oxidation of bidentate *OOCH is energy demanding and have proposed that monodentate *OOCH formed in pockets of bidentate *OOCH could be the active species.[6] This explanation would be in line with our findings, as the coverage of monodentate *OOCH would be too low and its residence time too short to be detected by *operando* SEIRAS.

At potentials less positive than 0.4 V *vs.* RHE, the appearance of the *COOH intermediate is accompanied by a fast decrease in the current, which suggests that C-bonded formic acid is more stable and difficult to oxidize compared to O-bonded formate. Finally, below 0.1 V *vs.* RHE, the simultaneous decrease in *COOH signals and increase in bridge *CO–*OH suggests that C-bonded formic acid is the active species for the formation of *CO. As the potential is increased again in the anodic scan (>0.2 V *vs.* RHE), formate oxidation is restored as shown by the current increase. However, this time the surface is covered by a combination of bridge and linear *CO, and formate oxidation proceeds through the indirect route, with lower reaction rates. Finally, positive of 0.55 V *vs.* RHE, *CO oxidation becomes thermodynamically favourable, and *CO (bridge and linear) is converted to CO_2. Above 0.7 V *vs.* RHE, the surface is rapidly poisoned by *OH adsorption, in combination with a sharp current decrease. It can also be observed that in all the measurements *CO bridge is formed first, reaches a plateau and is then slowly substituted by *CO linear. *CO linear only requires one adsorption site, as opposed to the bridged form which requires two. Therefore, we hypothesize that bridged *CO is the favoured species, which is converted to linear *CO at high coverages due to the limited availability of two adjacent sites for the formation of bridge *CO.

Elucidating the *CO formation mechanism

From Fig. 2, it appears clear that the decrease in reaction rate and the *CO bridge formation is faster in the hydrogen underpotential deposition (H_{UPD}) region of platinum, where we expect adsorbed *H is expected to be present on the terraces of Pt. This is in line with previous proposals suggesting that *CO formation can happen through a chemical disproportionation reaction, where the adsorbed formic acid reacts with hydrogen, to form water and *CO (*COOH + *H → *CO + H_2O).[3] This suggests that the ideal catalysts should destabilize *H, to avoid the formation of *CO, and that operating at low coverages of *H (positive of the the H_{UPD}) region should avoid the indirect oxidation pathway.

However, when performing formate oxidation in alkaline conditions at a lower scan rate of 2 mV s^{-1} (Fig. S1), one can notice the formation of *CO starting at potential as high as 0.5 V *vs.* RHE in the cathodic scan. Even though *CO formation still accelerates in the H_{UPD} region, this shows that *COOH disproportionation can happen at higher potentials, leading to the gradual poisoning of active sites. To elucidate the mechanism of *CO formation in alkaline pH we monitored the formation of reaction intermediates in CV scans, while gradually limiting the lower potential from the 0 V *vs.* RHE usually employed, to higher values. In fact, if disproportionation required the presence of adsorbed *H, one would expect that limiting the lower potential to 0.2 V *vs.* RHE would prevent the formation of *CO. The results are shown in Fig. 4.

As expected, if the potential is scanned all the way down to 0 V *vs.* RHE, *OOCH, *COOH, *CO bridge and *CO linear are formed. However, the formation of *CO bridge (following that of *COOH) is still observable when the lower potential is limited to 0.2 V *vs.* RHE and, to a small extent, even by stopping at 0.3 V *vs.* RHE. This shows that *CO can form at potentials above 0.3 V *vs.* RHE. Finally, if the potential is scanned between 0.4 and 1 V *vs.* RHE, only *OOCH is observed while both *COOH and *CO are absent. On top of confirming that *CO can form outside of the H_{UPD} region, these results suggest that disproportionation occurs only from the *COOH intermediate, in absence of which *CO is not detected. On the other hand, *OOCH leads to the fast and direct oxidation of formate. Therefore, we propose that the binding mode of formate controls the reaction pathway, with O-bonded and C-bonded formate causing respectively the direct and indirect oxidation of formate.

Another interesting observation is that the wavenumber at which *CO bridge and linear are detected shows a large redshift compared to ''pure'' CO, *i.e.* the case where CO gas is directly bubbled in the electrolyte. To illustrate this, Fig. 5a and b show the position of the formate-derived *CO intermediates as a function of potential (in blue), compared to the signal obtained

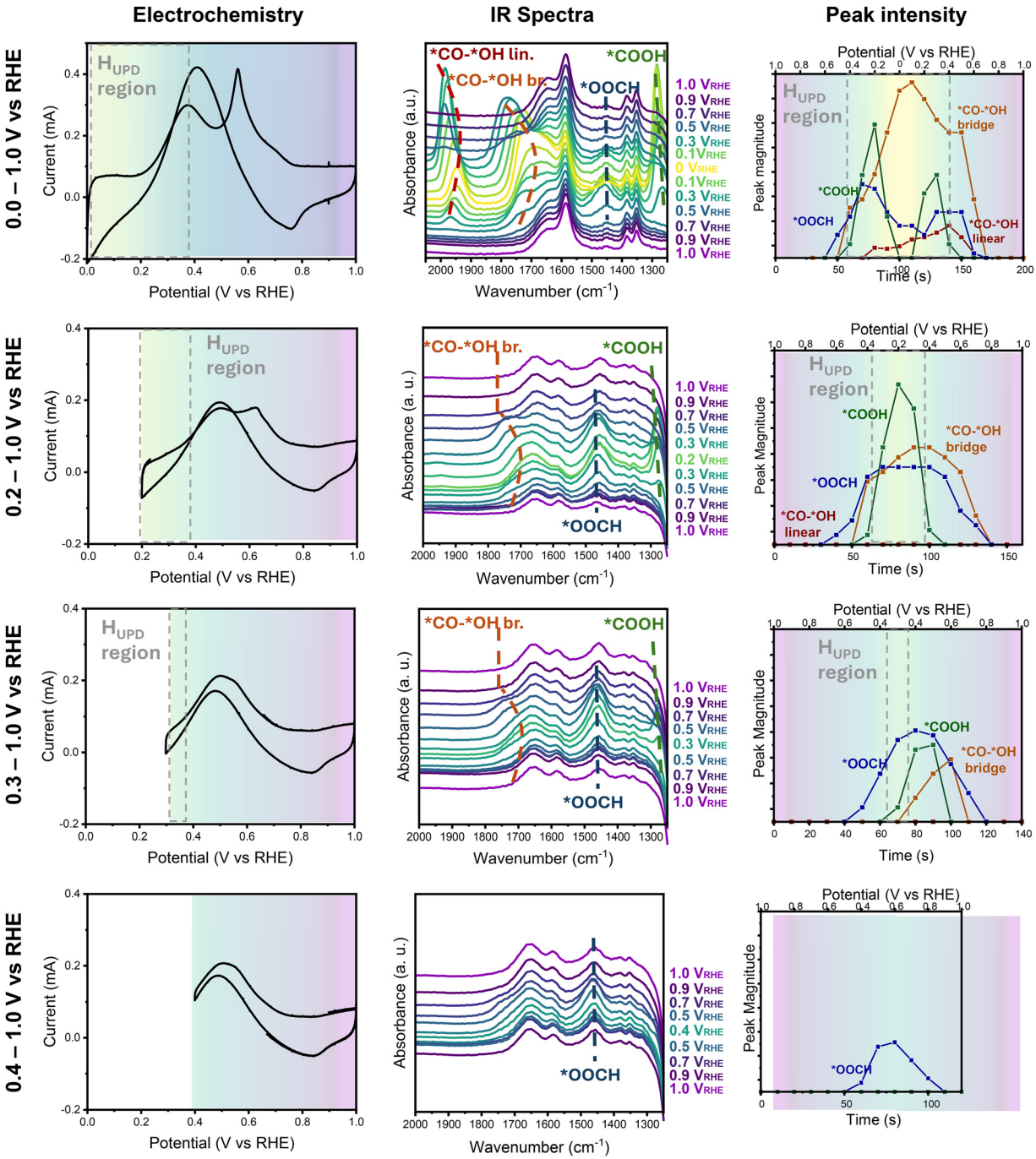

Fig. 4 From left to right are shown the electrochemical results of cyclic voltammograms, the corresponding SEIRAS spectra, and the magnitude of each SEIRAS peak as a function of time and applied potential. All the data were collected in 1 M NaOH with 1 M formate, at room temperature, with a scan rate of 10 mV s^{-1}, with an anodic potential limit of 1 V *vs.* RHE, and the cathodic limit increasing from the top to the bottom graph, between 0, 0.2, 0.3 and 0.4 V *vs.* RHE. The SEIRAS spectra shown in the second column are colour-coded to match the potential colour of the cyclic voltammogram, and are background-subtracted, with the background collected at OCP in 1 M NaOH.

from saturated CO gas at the same applied potential (shown in pink).

The values differ by up to 100 cm^{-1} and so does the potential dependency of the peak position. Linear and bridge-bound *CO from gaseous CO exhibits a typical potential dependence of ~60 cm^{-1} V^{-1}, known as the Stark tuning slope[30,31,43–45] and caused by: (i) electrostatic interactions between the electric field caused by the charged surface and the outer Helmholtz plane, and the dipole moment of the adsorbed *CO,[45] (ii) the compression or dissipation of the CO adsorbed layer,[44] and (iii) the change in *CO coverage.[43] On the contrary, the formate-derived linear *CO exhibits a potential dependence of

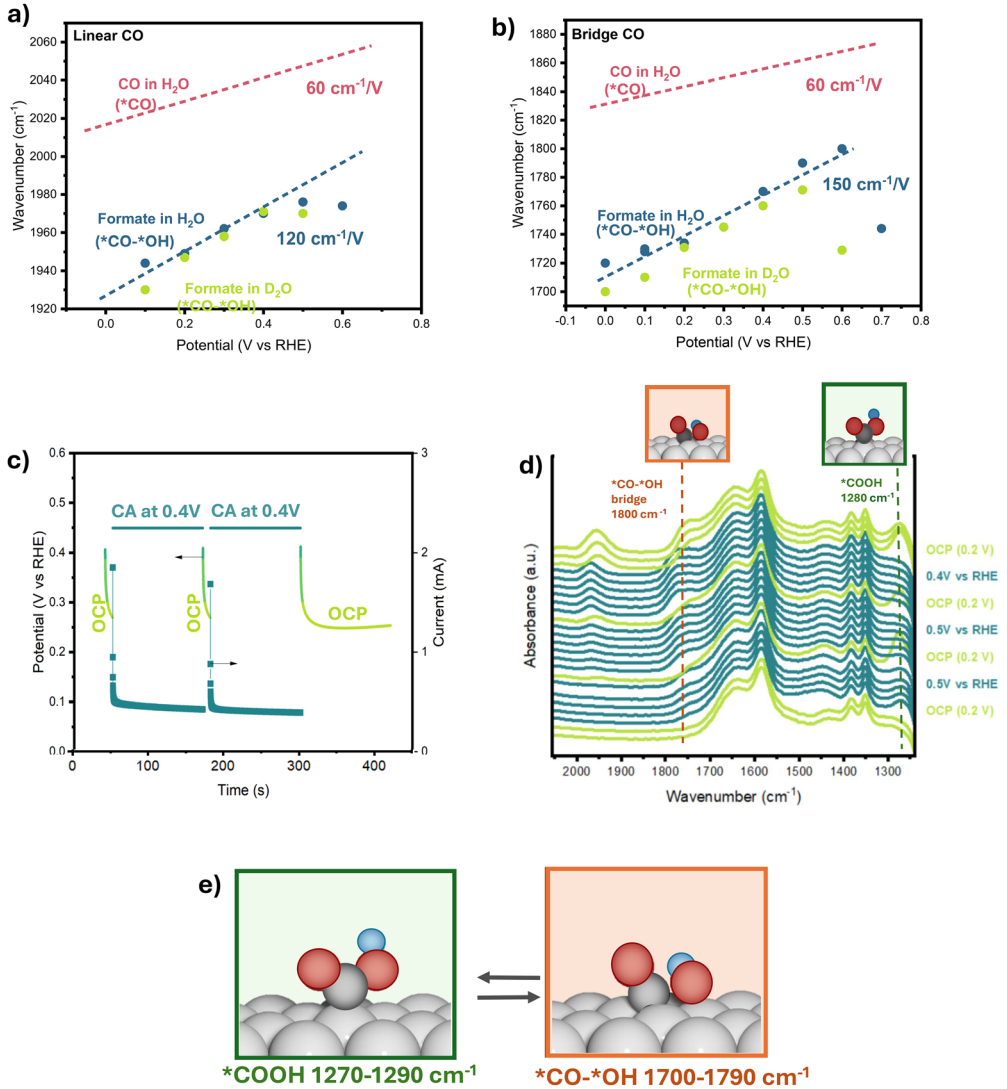

Fig. 5 (a) and (b) Show the peak position of formate-derived *CO linear and *CO bridge respectively, as a function of the applied potential. In pink are the results obtained in CO-saturated 0.1 M KOH (adapted from Katayama *et al.*). (c) and (d) Show the electrochemical and spectroscopic results of a potential step experiment performed in an *operando* SEIRAS cell, with polycrystalline Pt as working electrode, in 1 M NaOH with 1 M formate, at room temperature. (c) The potential is shown in a continuous line: the system started at OCP, then 0.45 V was applied for 2 min, then the system was left to relax to OCP for 10 s, followed by 2 min at 0.45 V and finally the system relaxes again to OCP. In the same graph is shown the measured current (reported as squared data points). (d) SEIRAS results for the step measurements, from the bottom to the top of the graph spectra are reported for increasing time, the spectra in light green are collected at 0.2 V *vs.* RHE, and those in blue were collected at OCP. (e) Schematic representation of the reversible *COOH → *CO–*OH step.

$\sim$120 cm^{-1} V^{-1} and bridged *CO shows an even higher value of $\sim$150 cm^{-1} V^{-1}. These values cannot be solely explained by the Stark effect associated with the electric field or changes in coverage.

We have reported this phenomenon before, in the context of methanol oxidation.[22] Similarly to what we observed here, methanol-derived *CO showed a red-shift of up to 60 cm^{-1} compared to pure *CO and displayed a potential dependence of $\sim$120 cm^{-1} V^{-1}. To test whether this shift originates from interactions with the electrolyte, or intermediates from the molecule of interest, we performed the same methanol oxidation experiments in deuterated electrolyte (1 M NaOD in D_2O). As expected, pure *CO showed negligible changes upon deuterium substitution. On the contrary, we reported a measurable shift of $\sim$20 cm^{-1} V^{-1} on methanol-derived *CO in the deuterated electrolyte, suggesting the presence of a partially hydrogenated *CO adsorbate, interacting with hydrogen from a hydroxy group. For the case of formate (Fig. 5), the red-shift compared to pure *CO indicates again the existence of *CO in a partially hydrogenated state but no significant shift is observed in the deuterated electrolyte. Therefore, we propose that *COOH degradation takes the form of *COOH → *CO–*OH, where *CO–*OH indicate the adsorption of *CO and *OH on contiguous Pt atoms, with a weak C–O bonding still existing between the C atom in *CO and the O atom in *OH, as shown in Fig. 5e. This mechanism would explain: (i) why *CO formation

can happen above H_{UPD}, (ii) the lower vibrational frequency of formate-derived *CO, compare to pure *CO, and (iii) why the first one does not change in deuterated electrolyte. Below 0.2 V *vs.* RHE, the *CO formation becomes faster, but all the observations remain valid, indicating that adsorbed *H facilitate *CO formation but is not directly involved in the reaction. Interestingly, the red-shift of *CO vibrational frequencies was not reported in acidic electrolyte,[2,13] for which *CO formation above 0.2 V *vs.* RHE was also not detected. This suggests that the mechanism of *CO formation is different in acidic (*COOH + *H → *CO + H_2O) and alkaline (*COOH → *CO–*OH) conditions, with only the first one requiring adsorbed protons. This observation could additionally explain the lower activity reported in alkaline electrolyte,[13] which on top of increasing competition with *OH, suffers from a slow but continuous formation of *CO species above H_{UPD}.

A similar *CO–*OH intermediate has been previously proposed by Herrero *et al.*, based uniquely on DFT studies of formic acid oxidation on platinum single crystals.[5] In their work, they suggest that *CO formation starts from monodentate formate (*OOCH), is followed by carbon adsorption on Pt to form *O–*COH and finally *CO–*OH, the same intermediate proposed here.

Another indication of the proposed *COOH → *CO–*OH mechanism in alkaline pH is shown in Fig. 5c and d. This shows the electrochemical and spectroscopical results of a step test where we applied a potential of 0.4 V *vs.* RHE for 2 minutes, and then left the system equilibrate to OCP for 10 seconds. At the start of the experiment the system is at OCP and no adsorbates are observed. When a potential of 0.4 V *vs.* RHE is applied, as expected, *COOH is formed and rapidly converted to *CO bridge. More surprisingly, if the potential control is stopped, the electrode reaches an open circuit potential of around 0.25 V, where *CO bridge is converted back to *COOH. This suggests that *COOH disproportionation is reversible and that the *OH co-produced in *CO formation remains weakly bound to *CO. It should be noted that alternative origins for the red-shifted *CO band are possible, including coverage effects, and electrostatic interactions. However, the absence of a comparable shift in acidic formic acid oxidation, the absence of an appreciable change in deuterated electrolyte, and the reversible nature of the *COOH disproportionation, prompt us to identify *CO–*OH as the most likely intermediate in alkaline conditions.

To confirm if the proposed *CO–*OH species would be stable, and consistent with the observed bands at 1700–1790 and 1930–1970 cm^{-1}, we also simulated the vibrational frequencies of bridge and linear *CO–*OH using DFT, and the results are summarized in Fig. 6.

We started from *COOH intermediate, which adsorbs monodentately *via* the C atom, with a C–OH bond length of 1.37 Å. By elongating the C–OH bond, bidentate adsorption *via* both C and O becomes possible but this significantly increases the energy. Thus, we systematically fixed the C–OH bond length at distance between 1.46 and 2.50 Å, extending from the stable *COOH structure (1.37 Å). After relaxation, *CO–*OH (bridge) structure was *meta*-stable from 1.80 to 2.50 Å, while *CO–*OH (linear) structure was *meta*-stable from 1.58 to 2.50 Å. *CO–*OH intermediate is always less stable than *COOH. This indicates that the conversion of *CO–*OH to *COOH is spontaneous in absence of an applied potential, as also observed experimentally (Fig. 5c–e). For comparison, *CO (bridge) and *CO (linear) were modeled by setting the C–OH bond length to a sufficiently large value (indicated as ∞ in Fig. 6), effectively removing the OH group and eliminating its interaction with CO. Frequencies of other vibrational modes and corresponding energies are provided in SI Tables S3–S5.

Fig. 6a summarizes the frequencies of C═O stretching of the simulated species, as a function of the C–OH bond length, starting from *COOH (in yellow), to *CO–*OH bridge to *CO bridge (in orange), and to *CO–*OH linear to *CO linear (in red). Shaded areas indicate experimental frequency ranges for *CO–*OH (bridge and linear) and *CO (bridge and linear). The color coding for the *COOH and *CO–*OH intermediates was selected to match that of other figures in the manuscript. The vibrational frequencies of *CO–*OH (bridge) are closer to

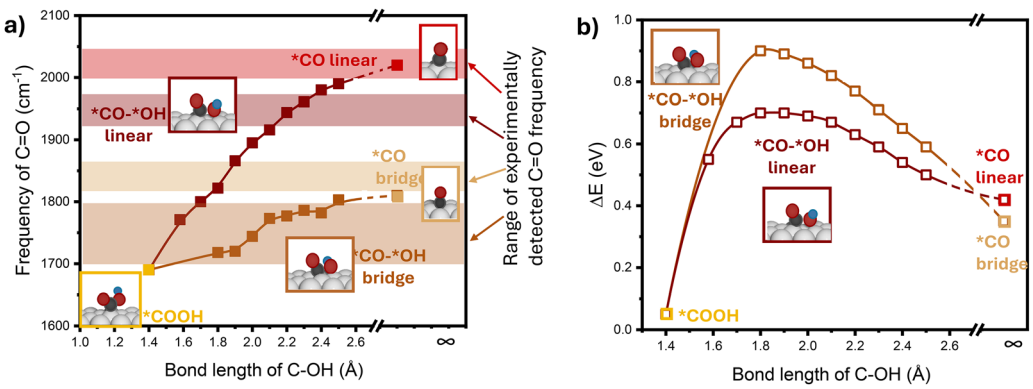

Fig. 6 Calculated C═O asymmetric stretching frequencies (cm^{-1}) (a) and DFT energy differences (ΔE/eV, referenced to *COOH = 0 eV) (b) as functions of C–OH bond length for intermediates *COOH, *CO–*OH (bridge), *CO–*OH (linear), *CO (bridge), and *CO (linear). Color coding matches Fig. 3. A C–OH bond length of ∞ represents fully separated CO and OH groups. Experimental ranges for *CO–*OH (bridge), *CO–*OH (linear), *CO bridge and *CO linear are shown as shaded areas; all other points are from DFT.

those of *COOH than those of *CO–*OH (linear), suggesting greater structural similarity. However, the DFT-calculated energy differences (ΔE, relative to *COOH = 0 eV) indicate that the bridge configuration is less stable than the linear one. These ΔE values are plotted in Fig. 6b. For *CO–*OH (bridge), DFT frequencies align with experimental data when the C–OH bond length is 1.80–2.40 Å, corresponding to ΔE of 0.65–0.90 eV. For *CO–*OH (linear), agreement occurs at C–OH bond lengths of 2.20–2.30 Å at an energy cost of ΔE between 0.59–0.63 eV. At these bond lengths, the vibrational frequencies of bridged and linear *CO–*OH species is $\approx$100 cm^{-1} lower than the prediction of *CO, matching the experimental difference between "pure" *CO and formate-derived *CO. However, energetically, neither intermediate appears stable enough to be a detectable species from *COOH to *CO. Their experimental observability may arise from solvation effects not included in our calculations, where water molecules could help stabilize these intermediates.

Conclusion

Previous studies of formic acid oxidation on Pt have concluded that: (i) the reaction can proceed through a direct and indirect pathway, (ii) indirect oxidation leads to the formation of *CO, which poisons the surface, and (iii) at high potentials ($>$0.6 V *vs.* RHE) activity drops as a result of *OH adsorption. However, the active species prior to direct oxidation to CO_2 are still the subject of debate, as summarized in Fig. 1, with reports proposing monodentate *OOCH, bidentate *OOCH, *COOH or formic acid as the active species. Regarding the indirect activation pathway, most works propose that *CO is formed through a disproportionation reaction, where *COOH reacts with protons to form *CO and water. However, most mechanistic insights are derived from DFT calculations and the only intermediates that have been experimentally observed are bidentate formate and *CO.

Here, *operando* surface-enhanced infrared absorption spectroscopy is used to directly probe surface intermediates during formate oxidation on Pt in alkaline media. Two distinct formate-derived adsorbates are resolved. At potentials above 0.4 V *vs.* RHE, stable oxidation currents are observed without hysteresis, and bidentate *OOCH is the only detectable surface species, indicating that oxygen-bound formate dominates under conditions favouring direct oxidation. In contrast, at lower potentials a second intermediate emerges, characterized by a band at 1270–1290 cm^{-1}. This species appears exclusively under conditions that lead to *CO formation and is absent when direct oxidation is stable.

Based on its potential dependence, its strict correlation with *CO formation, and comparison with prior mechanistic and computational studies, this intermediate is most consistently assigned to a carbon-bound formate-derived species, commonly described as *COOH. Although *COOH has been widely proposed as the precursor to *CO formation, it has not previously been observed experimentally by SEIRAS. Its absence in earlier studies is plausibly attributed to its short lifetime and to surface-selection rules. In the present work, the combination of high formate concentration and high alkali cation concentration in alkaline electrolyte likely stabilizes this species and enhances its spectroscopic visibility.

Formate-derived *CO formed in alkaline media exhibits a pronounced red-shift of $\approx$100 cm^{-1}, compared to "pure" *CO (generated by direct CO adsorption). Isotopic substitution experiments exclude electrolyte effects as the origin of this

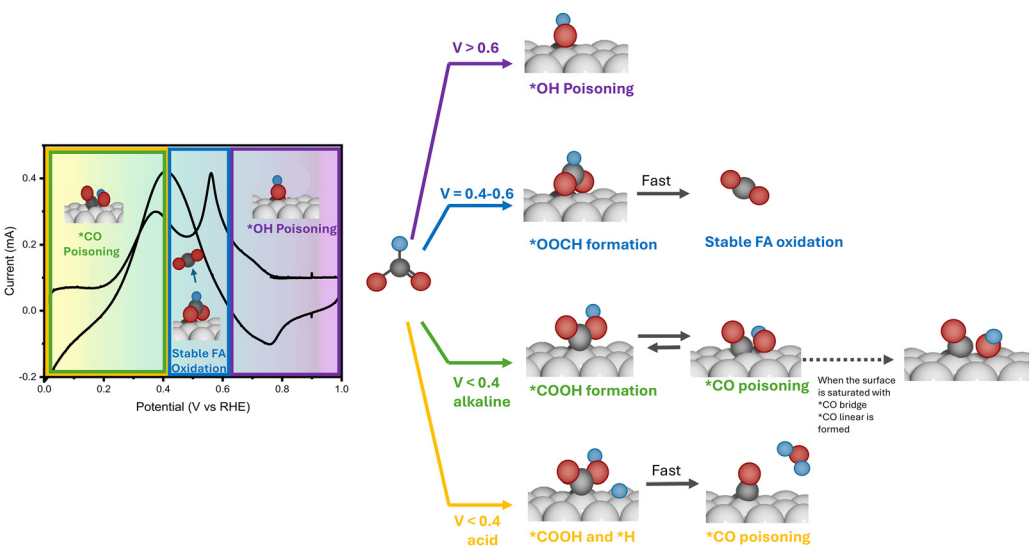

Fig. 7 Summary of the reaction pathway proposed in this work. Above 0.4 V *vs.* RHE, bi-dentate formate (*OOCH) is adsorbed *via* the oxygen atom, leading to the fast and stable direct oxidation to CO_2. Below 0.4 V *vs.* RHE, formate adsorbs *via* the carbon atom (*COOH). This adsorption configuration leads to the formation of *CO and the gradual poisoning of the catalyst. In acidic media, as previously reported, *COOH oxidation to *CO requires the presence of protons. On the contrary, in this work, we have shown that in alkaline media *COOH oxidation proceeds *via* a *CO–*OH intermediate, which can form in absence of protons.

shift. Instead, DFT calculations and chronoamperometric measurements support an alkaline-specific mechanism in which *CO formed *via* C-bound intermediates is weakly stabilized through interaction with adjacent *OH species (Fig. 7). Upon relaxation to open-circuit potential, this species is reversibly converted back to the carbon-bound intermediate.

The mechanism summarized in Fig. 7 allows us to deduce design criteria for active formate oxidation catalysts. Since the *OOCH and *COOH intermediates catalyze respectively the direct and indirect oxidation of formate, our results indicate that suppressing CO formation requires stabilizing oxygen-bound formate adsorption. Because *OOCH and *COOH binding energies are not intrinsically correlated,[21] selective suppression of *CO formation is, in principle, achievable through catalyst and electrolyte design; although scaling relations with *OH adsorption constrain the accessible potential window in alkaline media.[21] Beyond Pt, this work suggests that metals or alloying material that preferentially stabilize O-bound carboxylates over C-bound species should suppress *CO formation. Furthermore, our findings suggest that cations might play a role in stabilizing certain intermediates through electrostatic interactions. This means that electrolyte engineering could be an effective approach to control reaction mechanisms, but this remains to be confirmed by more focused studies on cation effects.

Beyond formic acid oxidation, the identification of these intermediates provides a spectroscopic reference for more complex biomass oxidation reactions, in which CO poisoning remains a critical limitation. Although the specific mechanistic details identified here may not directly translate to systems involving larger and more complex reactants, the present results highlight the importance of carefully analyzing shifts in the *CO vibrational band, as such variations may contain mechanistic information about the pathway of *CO formation. Given that formate is a common intermediate in biomass oxidation networks, these findings may also aid in the identification of formate-derived surface species and in understanding the factors governing complete oxidation to CO_2. More generally, this work demonstrates that adsorption geometry and electrolyte composition play decisive roles in determining reaction pathways and poisoning mechanisms in electrocatalytic oxidation reactions.

Experimental

Electrocatalysts preparation

Operando SEIRAS measurements were performed using a Si hemisphere (radius 22 mm from Pier optics), on which an enhancement layer of Pd was deposited, followed by a thin film of Pt. The preparation method is described elsewhere.[22,46] In brief, the Si surface was prepared by dropcasting 1 mL of 40% NH_4F solution for a minute. Subsequently, palladium was depositing by drop-casting a solution of 1% HF–1 mM $PdCl_2$ for 5 min at room temperature. Finally, platinum was deposited by immersing the Si hemisphere in a Pt plating solution for 5 minutes, at 50 °C. The plating solution was obtained by mixing 30 mL of LECTROLESS Pt 100 basic solution (30 mL, Electroplating Engineering of Japan Ltd), 8 mL of 28% NH_3 solution, and ultrapure water.

SEIRAS measurement

The Si prism was mounted on an in-house developed electrochemical cell, featuring a Pt rod counter electrode and Hg/HgO reference. All the measurements were performed in either 1 M NaOH or 1 M formate, 1 M NaOH. The SEIRAS spectra were obtained with an FTIR Nicolet iS50 (Thermo Fisher Scientific) spectrometer equipped with a Mercury–Cadmium–Telluride (MCT) detector. The optical path was fully replaced with N_2 gas. The measurements were performed with a 4 cm^{-1} resolution in the 500–4000 cm^{-1} spectral range; 32 scans were averaged, giving a spectral collection every 10 s. The SEIRAS spectra were recorded using a custom-made single reflection ATR optics system at an incident angle of 67°. For the isotopically labelled experiments, 1 M NaOD (99.5% from Merck) in D_2O (99.9% from Merck) was used.

Before each experiment, nitrogen was bubbled in 1 M NaOH or 1 M NaOD for 15 minutes to remove oxygen. Then the Pt surface was cleaned by performing 10 cyclic voltammograms between 0 and 1 V *vs.* RHE, at 20 mV s^{-1}. The system was then left to equilibrate at open circuit potential and a spectrum was recorded as reference. 1 M Formate was subsequently added to the electrolyte and the experiment started. All the resulting spectra are shown as absorbance *vs.* potential (in V *vs.* RHE). Absorbance units are defined as $\log(I_0/I)$ where I_0 and I represent the reference spectra and the spectra of interest respectively.

Computational details

We use density functional theory (DFT) to calculate energies and frequencies of possible formic acid oxidation intermediates. We model adsorption of intermediates using a face-centered cubic (FCC) Pt slab with a $p(4 \times 4)$ (111) surface cell and 4 atomic layer thickness. The 2 bottom layers are fixed to emulate bulk metal. To avoid interlayer interactions, the distance between metal slabs (periodic images) is set to 17 Å. Atomic simulation environment (ASE) program[47] was employed for the atomic structures. GPAW program,[48,49] was employed for DFT calculations with revised Perdew–Burke–Ernzerhof exchange–correlation functional,[50] 400 eV energy cutoff for plane-wave basis sets and $4 \times 4 \times 1$ Monkhorst–Pack *k*-point sampling. The maximum force on each atom is set to 0.03 eV $Å^{-1}$ for relaxed atomic structures and frequencies. We stress that the calculations do not account for solvation of the *COOH, *CO–*OH, or *CO species, because including solvation effects are computationally expensive.[51] It is possible that the solvation effects are similar for the different species and therefore cancel out to some extent, but the lack of solvation effects could perhaps also explain some of the discrepancies between modeling and experimental observations.

Conflicts of interest

There are no conflicts to declare.

Data availability

The electrochemistry and spectroscopy data supporting this article are provided in the supplementary information (SI). The DFT calculations and python scripts are accessible online at: https://erda.ku.dk/archives/d57d50eea957e20eb94a73a5d770bb51/published-archive.html.

Supplementary information (SI) is available. See DOI: https://doi.org/10.1039/d6ey00007j.

Acknowledgements

S. F. acknowledges the RSC collaboration grant C23-0818957162, and the Engineering and Physical Sciences Research Council (EPSRC) program grant EP/W031019. I. E. L. S. acknowledges the Royce Institute (EP/P02520X/1). Y. K. acknowledges the financial support by the Japan Society for the Promotion of Science (JSPS) KAKENHI Grant Number 25K01880 and by the Japan Science and Technology Agency (JST) under the Adopting Sustainable Partnerships for Innovative Research Ecosystem (ASPIRE) program (grant no JPMJAP2422). Z. M., H. H. K., and J. R. acknowledge financial support from the Independent Research Fund Denmark grant no. 1127-00372B and the Danish National Research Foundation, Center for High Entropy Alloy Catalysis (CHEAC) DNRF149.

References

1 J. Scaranto and M. Mavrikakis, HCOOH decomposition on Pt(111): a DFT study, *Surf. Sci.*, 2016, **648**, 201–211, DOI: 10.1016/j.susc.2015.09.023.
2 G. Samjeské, A. Miki, S. Ye and M. Osawa, Mechanistic Study of Electrocatalytic Oxidation of Formic Acid at Platinum in Acidic Solution by Time-Resolved Surface-Enhanced Infrared Absorption Spectroscopy, *J. Phys. Chem. B*, 2006, **110**(33), 16559–16566, DOI: 10.1021/jp061891l.
3 A. Bagger, K. D. Jensen, M. Rashedi, R. Luo, J. Du and D. Zhang, *et al.*, Correlations between experiments and simulations for formic acid oxidation, *Chem. Sci.*, 2022, **13**(45), 13409–13417, DOI: 10.1039/d2sc05160e.
4 T. Yang, S. Hou, J. Xing, C. Liu, J. Ge and W. Xing, Formic acid electro-oxidation: mechanism and electrocatalysts design, *Nano Res.*, 2023, **16**(3), 3607–3621, DOI: 10.1007/s12274-022-4319-1.
5 E. Herrero and J. M. Feliu, Understanding formic acid oxidation mechanism on platinum single crystal electrodes, *Curr. Opin. Electrochem.*, 2018, **9**, 145–150, DOI: 10.1016/j.coelec.2018.03.010.
6 A. Ferre-Vilaplana, J. V. Perales-Rondón, C. Buso-Rogero, J. M. Feliu and E. Herrero, Formic acid oxidation on platinum electrodes: a detailed mechanism supported by experiments and calculations on well-defined surfaces, *J. Mater. Chem. A*, 2017, **5**(41), 21773–21784, DOI: 10.1039/c7ta07116g.
7 A. Cuesta, G. Cabello, C. Gutiérrez and M. Osawa, Adsorbed formate: the key intermediate in the oxidation of formic acid on platinum electrodes, *Phys. Chem. Chem. Phys.*, 2011, **13**(45), 20091–20095, DOI: 10.1039/c1cp22498k.
8 A. Cuesta, G. Cabello, M. Osawa and C. Gutiérrez, Mechanism of the electrocatalytic oxidation of formic acid on metals, *ACS Catal.*, 2012, **2**(5), 728–738, DOI: 10.1021/cs200661z.
9 J. Xu, D. Yuan, F. Yang, D. Mei, Z. Zhang and Y. X. Chen, On the mechanism of the direct pathway for formic acid oxidation at a Pt(111) electrode, *Phys. Chem. Chem. Phys.*, 2013, **15**(12), 4367–4376, DOI: 10.1039/c3cp44074e.
10 V. Grozovski, V. Climent, E. Herrero and J. M. Feliu, Intrinsic activity and poisoning rate for HCOOH oxidation on platinum stepped surfaces, *Phys. Chem. Chem. Phys.*, 2010, **12**(31), 8822–8831, DOI: 10.1039/b925472b.
11 W. Gao, J. A. Keith, J. Anton and T. Jacob, Theoretical elucidation of the competitive electro-oxidation mechanisms of formic acid on Pt(111), *J. Am. Chem. Soc.*, 2010, **132**(51), 18377–18385, DOI: 10.1021/ja1083317.
12 M. Osawa, K. I. Komatsu, G. Samjeské, T. Uchida, T. Ikeshoji and A. Cuesta, *et al.*, The role of bridge-bonded adsorbed formate in the electrocatalytic oxidation of formic acid on platinum, *Angew. Chem., Int. Ed.*, 2011, **50**(5), 1159–1163, DOI: 10.1002/anie.201004782.
13 J. Joo, T. Uchida, A. Cuesta, M. T. M. Koper and M. Osawa, The effect of pH on the electrocatalytic oxidation of formic acid/formate on platinum: a mechanistic study by surface-enhanced infrared spectroscopy coupled with cyclic voltammetry, *Electrochim. Acta*, 2014, **129**, 127–136, DOI: 10.1016/j.electacta.2014.02.040.
14 H. F. Wang and Z. P. Liu, Formic acid oxidation at Pt/H_2O interface from periodic DFT calculations integrated with a continuum solvation model, *J. Phys. Chem. C*, 2009, **113**(40), 17502–17508, DOI: 10.1021/jp9059888.
15 H. Ye, S. Favero, H. Tyrrell, K. Plub-in, A. Hankin and R. R. Rao, *et al.*, Progress and Challenges in Electrochemical Glycerol Oxidation: The Importance of Benchmark Methods and Protocols, *ChemCatChem*, 2025, **17**, e00152, DOI: 10.1002/cctc.202500152.
16 J. V. Perales-Rondón, E. Herrero and J. M. Feliu, Effects of the anion adsorption and pH on the formic acid oxidation reaction on Pt(111) electrodes, *Electrochim. Acta*, 2014, **140**, 511–517, DOI: 10.1016/j.electacta.2014.06.057.
17 H. F. Wang and Z. P. Liu, Formic acid oxidation at Pt/H_2O interface from periodic DFT calculations integrated with a continuum solvation model, *J. Phys. Chem. C*, 2009, **113**(40), 17502–17508, DOI: 10.1021/jp9059888.
18 M. D. Macia, E. Herrero, J. M. Feliu and A. Aldaz, Formic acid self-poisoning on bismuth-modified Pt(755) and Pt(775) electrodes, *Electrochem. Commun.*, 1999, **1**, 87–89.
19 H. Kita and H. W. Lei, Oxidation of formic acid in acid solution on Pt single-crystal electrodes, *J. Electroanal. Chem.*, 1995, **388**, 167–177.
20 M. D. Maciá, E. Herrero and J. M. Feliu, Formic acid self-poisoning on adatom-modified stepped electrodes, *Electrochim. Acta*, 2002, **47**(47), 3653–3661Available from.
21 V. Grozovski, V. Climent, E. Herrero and J. M. Feliu, Intrinsic activity and poisoning rate for HCOOH oxidation at

Pt(100) and vicinal surfaces containing monoatomic (111) steps, *ChemPhysChem*, 2009, **10**(11), 1922–1926, DOI: 10.1002/cphc.200900261.

22 Y. Katayama, R. Kubota, R. R. Rao, J. Hwang, L. Giordano and A. Morinaga, *et al.*, Direct Observation of Surface-Bound Intermediates during Methanol Oxidation on Platinum under Alkaline Conditions, *J. Phys. Chem. C*, 2021, **125**(48), 26321–26331, DOI: 10.1021/acs.jpcc.1c06878.

23 J. F. Gomes, C. A. Martins, M. J. Giz, G. Tremiliosi-Filho and G. A. Camara, Insights into the adsorption and electro-oxidation of glycerol: self-inhibition and concentration effects, *J. Catal.*, 2013, **301**, 154–161, DOI: 10.1016/j.jcat.2013.02.007.

24 W. Chen, L. Zhang, L. Xu, Y. He, H. Pang and S. Wang, *et al.*, Pulse potential mediated selectivity for the electrocatalytic oxidation of glycerol to glyceric acid, *Nat. Commun.*, 2024, **15**, 2420, DOI: 10.1038/s41467-024-46752-4.

25 R. M. L. M. Sandrini, J. Renata, E. Herrero and J. M. Feliu, Mechanistic aspects of glycerol electrooxidation on Pt(111) electrode in alkaline media, *Electrochem. Commun.*, 2018, **86**, 149–152, DOI: 10.1016/j.elecom.2017.11.027.

26 G. A. B. Mello, W. Cheuquepán, V. Briega-Martos and J. M. Feliu, Glucose electro-oxidation on Pt(100) in phosphate buffer solution (pH 7): a mechanistic study, *Electrochim. Acta*, 2020, 354, DOI: 10.1016/j.electacta.2020.136765.

27 M. P. J. M. van der Ham, E. van Keulen, M. T. M. Koper, A. A. Tashvigh and J. H. Bitter, Steering the Selectivity of Electrocatalytic Glucose Oxidation by the Pt Oxidation State, *Angew. Chem., Int. Ed.*, 2023, **62**(33), e202306701, DOI: 10.1002/anie.202306701.

28 L. Pérez-Martínez, L. M. Machado de los Toyos, J. J. T. Shibuya and A. Cuesta, Methanol dehydrogenation on Pt electrodes: active sites and role of adsorbed spectators revealed through time-resolved ATR-SEIRAS, *ACS Catal.*, 2021, **11**(21), 13483–13495, DOI: 10.1021/acscatal.1c03870.

29 R. ShyamYadav, M. G. Gebru, H. Teller, A. Schechter and H. Kornweitz, The origins of formic acid electrooxidation on selected surfaces of Pt, Pd, and their alloys with Sn, *J. Mater. Chem. A*, 2024, **12**(6), 3311–3322, DOI: 10.1039/d3ta07219c.

30 Y. G. Yan, Q. X. Li, S. J. Huo, M. Ma, W. B. Cai and M. Osawa, Ubiquitous strategy for probing ATR surface-enhanced infrared absorption At platinum group metal-electrolyte interfaces, *J. Phys. Chem. B*, 2005, **109**(16), 7900–7906, DOI: 10.1021/jp044085s.

31 B. B. Blizanac, M. Arenz, P. N. Ross and N. M. Markovic, Surface electrochemistry of CO on reconstructed gold single crystal surfaces studied by infrared reflection absorption spectroscopy and rotating disk electrode, *J. Am. Chem. Soc.*, 2004, **126**(32), 10130–10141, DOI: 10.1021/ja049038s.

32 Z. Fang and W. Chen, Recent advances in formic acid electro-oxidation: from the fundamental mechanism to electrocatalysts, *Nanoscale Adv.*, 2021, **3**(1), 94–105, DOI: 10.1039/d0na00803f.

33 J. John, H. Wang, E. D. Rus and D. Abrun, Mechanistic Studies of Formate Oxidation on Platinum in Alkaline Medium, *J. Phys. Chem. C*, 2012, **116**, 5810–5820.

34 G. Samjeske, Mechanistic Study of Electrocatalytic Oxidation of Formic Acid at Platinum in Acidic Solution by Time-Resolved Surface-Enhanced Infrared Absorption Spectroscopy, *J. Phys. Chem. B*, 2006, **110**(110), 16559–16566.

35 I. J. McPherson, P. A. Ash, R. M. J. Jacobs and K. A. Vincent, Formate adsorption on Pt nanoparticles during formic acid electro-oxidation: insights from: in situ infrared spectroscopy, *Chem. Commun.*, 2016, **52**(85), 12665–12668, DOI: 10.1039/c6cc05955d.

36 B. S. Beckingham, N. A. Lynd and D. J. Miller, Monitoring multicomponent transport using in situ ATR FTIR spectroscopy, *J. Membr. Sci.*, 2018, **550**, 348–356, DOI: 10.1016/j.memsci.2017.12.072.

37 C. Lucks, A. Rossberg, S. Tsushima, H. Foerstendorf, K. Fahmy and G. Bernhard, Formic acid interaction with the uranyl(VI) ion: structural and photochemical characterization, *Dalton Trans.*, 2013, **42**(37), 13584–13589, DOI: 10.1039/c3dt51711j.

38 S. C. Edington, A. Gonzalez, T. R. Middendorf, D. B. Halling, R. W. Aldrich and C. R. Baiz, Coordination to lanthanide ions distorts binding site conformation in calmodulin, *Proc. Natl. Acad. Sci. U. S. A.*, 2018, **115**(14), E3126–E3134, DOI: 10.1073/pnas.1722042115.

39 C. O. Areán, M. R. Delgado, K. Frolich, R. Bulánek, A. Pulido and G. F. Bibiloni, *et al.*, Computational and Fourier transform infrared spectroscopic studies on carbon monoxide adsorption on the zeolites Na-ZSM-5 and K-ZSM-5: evidence of dual-cation sites, *J. Phys. Chem. C*, 2008, **112**(12), 4658–4666, DOI: 10.1021/jp7109934.

40 J. Joo, T. Uchida, A. Cuesta, M. T. M. Koper and M. Osawa, The effect of pH on the electrocatalytic oxidation of formic acid/formate on platinum: A mechanistic study by surface-enhanced infrared spectroscopy coupled with cyclic voltammetry, *Electrochim. Acta*, 2014, **129**, 127–136, DOI: 10.1016/j.electacta.2014.02.040.

41 P. J. Feibelman, B. Hammer, J. K. Norskov, F. Wagner, M. Scheffler and R. Stump, *et al.*, The CO/Pt(111) Puzzle A, *J. Phys. Chem. B*, 2001, **105**(18), 4018–4025, DOI: 10.1021/jp002302t.

42 I. Grinberg, Y. Yourdshahyan and A. M. Rappe, CO on Pt(111) puzzle: a possible solution, *J. Chem. Phys.*, 2002, **117**(5), 2264–2270, DOI: 10.1063/1.1488596.

43 J. Uddin and A. B. Anderson, Trends with coverage and pH in Stark tuning rates for CO on Pt(111) electrodes, *Electrochim. Acta*, 2013, **108**, 398–403, DOI: 10.1016/j.electacta.2013.06.088.

44 D. K. Lambert, Vibrational Stark Effect of Adsorbates at Electrochemical Interfaces, *Electrochim. Acta*, 1996, **41**(5), 623–630.

45 V. Stamenkovic, K. C. Chou, G. A. Somorjai, P. N. Ross and N. M. Markovic, Vibrational properties of CO at the Pt(111)-solution interface: the anomalous stark-tuning slope, *J. Phys. Chem. B*, 2005, **109**(2), 678–680, DOI: 10.1021/jp044802i.

46 Y. Katayama, L. Giordano, R. R. Rao, J. Hwang, H. Muroyama and T. Matsui, *et al.*, Surface (Electro)chemistry

of CO_2 on Pt Surface: an in Situ Surface-Enhanced Infrared Absorption Spectroscopy Study, *J. Phys. Chem. C*, 2018, **122**(23), 12341–12349, DOI: 10.1021/acs.jpcc.8b03556.

47 A. Hjorth Larsen, J. JØrgen Mortensen, J. Blomqvist, I. E. Castelli, R. Christensen and M. Dułak, *et al.*, The atomic simulation environment – A Python library for working with atoms, *J. Phys.: Condens. Matter*, 2017, **29**(27), 273002, DOI: 10.1088/1361-648X/aa680e.

48 J. Enkovaara, C. Rostgaard, J. J. Mortensen, J. Chen, M. Dułak and L. Ferrighi, *et al.*, Electronic structure calculations with GPAW: a real-space implementation of the projector augmented-wave method, *J. Phys.: Condens. Matter*, 2010, **22**(25), 253202, DOI: 10.1088/0953-8984/22/25/253202.

49 J. J. Mortensen, L. B. Hansen and K. W. Jacobsen, Real-space grid implementation of the projector augmented wave method, *Phys. Rev. B: Condens. Matter Mater. Phys.*, 2005, **71**(3), 035109, DOI: 10.1103/PhysRevB.71.035109.

50 B. Hammer, L. B. Hansen and J. K. No, Improved adsorption energetics within density-functional theory using revised Perdew–Burke–Ernzerhof functionals, *Phys. Rev. B: Condens. Matter Mater. Phys.*, 1999, **59**(11), 7413–7421.

51 H. H. Heenen, J. A. Gauthier, H. H. Kristoffersen, T. Ludwig and K. Chan, Solvation at metal/water interfaces: An ab initio molecular dynamics benchmark of common computational approaches, *J. Chem. Phys.*, 2020, **152**(14), 144703, DOI: 10.1063/1.5144912.